Quantitative study of microplastic degradation in urban hydrosystems: comparing in-situ environmentally aged microplastics vs. artificially aged materials generated via accelerated photo-oxidation

Okba Mostefaoui, Zoé Iannuzzi, Diego Lopez, Emmanuel Mignot, Gislain Lipeme Kouyi, Rémy Bayard, Valérie Massardier-Nageotte, Brice Mourier

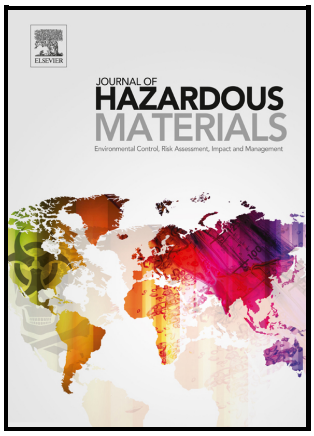

Quantitative study of microplastic degradation in urban hydrosystems: comparing in-situ environmentally aged microplastics vs. artificially aged materials generated via accelerated photo-oxidation

Okba Mostefaoui, Zoe Iannuzzi, Diego Lopez, Emmanuel Mignot, Gislain Lipeme Kouyi, Rémy Bayard, Valérie Massardier-Nageotte, Brice Mourier

PII: S0304-3894(24)03668-9

DOI: https://doi.org/10.1016/j.jhazmat.2024.137087

Reference: HAZMAT137087

To appear in: *Journal of Hazardous Materials*

Received date: 20 May 2024
Revised date: 27 November 2024
Accepted date: 31 December 2024

Please cite this article as: Okba Mostefaoui, Zoe Iannuzzi, Diego Lopez, Emmanuel Mignot, Gislain Lipeme Kouyi, Rémy Bayard, Valérie Massardier-Nageotte and Brice Mourier, Quantitative study of microplastic degradation in urban hydrosystems: comparing in-situ environmentally aged microplastics vs. artificially aged materials generated via accelerated photo-oxidation, *Journal of Hazardous Materials,* (2025) doi:https://doi.org/10.1016/j.jhazmat.2024.137087

Quantitative study of microplastic degradation in urban hydrosystems: comparing in-situ environmentally aged microplastics vs. artificially aged materials generated via accelerated photo-oxidation

Okba Mostefaoui[a,b,*], Zoe Iannuzzi[c,d,*], Diego Lopez[a], Emmanuel Mignot[a], Gislain Lipeme Kouyi[d], Rémy Bayard[d], Valérie Massardier-Nageotte[b], Brice Mourier[c]

[a]*INSA Lyon, CNRS, Ecole Centrale de Lyon, Univ Claude Bernard Lyon 1, LMFA, UMR5509 69621, Villeurbanne, France*

[b]*Université Claude Bernard Lyon 1, INSA Lyon, Université Jean Monnet, CNRS UMR 5223, Ingénierie des Matériaux Polymères F-69621, Villeurbanne cedex, France*

[c]*ENTPE, Université Claude Bernard Lyon 1, CNRS, UMR 5023 LEHNA 69518, Vaulx-en-Velin Cedex, 3 Rue M. Audin France*

[d]*INSA Lyon, DEEP, UR7429 69621, Villeurbanne, France*

Abstract

The degradation of plastic waste is a major research challenge due to the adverse impacts of microplastic weathering on the environment and ecosystems. As a major source of plastic contamination comes from urban hydrosystems, studying MP degradation prior to their environmental dissemination is crucial. Through a combination of field sampling and laboratory experiments, this study provides a thorough statistical degradation comparison analysis between polyethylene in situ environmentally aged microplastics and artificially aged films. In the laboratory, pristine nonadditivated low-density polyethylene films were exposed to controlled ultraviolet (UV) radiation to simulate aging for various durations. Firstly, the study aims to assess the representativeness of controlled UV degradation to mimic urban in-situ MPs. The second goal is to identify polyethylene (PE) degradation characteristics in various environmental matrices such as stormwater, suspended solids and sediment samples from a stormwater detention basin in a large urban area in France. Artificially aged plastics exhibit distinct alterations in physical and chemical properties, corresponding solely to the abiotic degradation observed in-situ. In contrast, environmental particles display notable markers of biotic chemical degradation and hydrolysis. Moreover, the degradation environment varies significantly: it is predominantly abiotic for MPs collected in stormwater samples, while it is largely biotic for MPs collected in sediment and suspended solid samples. Besides, MPs from stormwater

and suspended solid samples show a higher degree of hydrolysis degradation. Finally, additional comparisons with common consumer materials, before and after use, show almost no signs of notable degradation compared to the environmentally and artificially aged materials considered in this study.

Graphical abstract

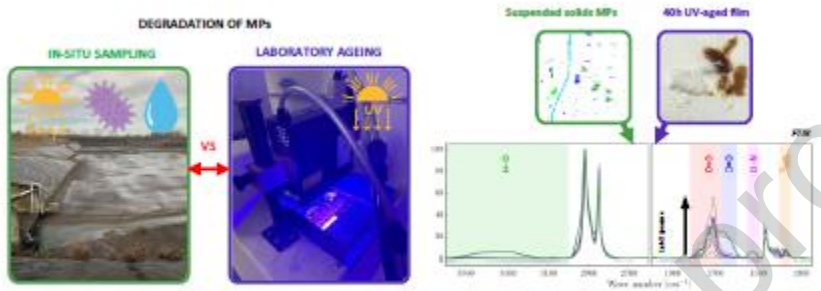

Environmental Implication

Hazardous risks linked to microplastic degradation are a significant concern in every urban system. Our study addresses this issue by developing an integrated approach to understand polyethylene degradation in both real-world and controlled laboratory settings. Through this approach, the proportion of biotic degradation is estimated relative to abiotic degradation. Studying polyethylene transfer in urban hydrosystems allows assessment of the critical degradation phases of this polymer in the environment and the formulation of effective mitigation strategies. The integration of laboratory results enables recommendations on aging processes for experimental researchers, in particular to carry out representative degradation studies of microplastics in situ.

Keywords: Polyethylene; Stormwater; Environmental aging; FTIR; NMR

1. Introduction

The ubiquitous presence of microplastics (MPs) in the environment poses significant risks to ecosystems and human health (Wang et al., 2019; Winiarska et al., 2024; Hanun et

al., 2021), notably due to the colonization of microorganisms and the aggregation of micropollutants (Wilkinson et al., 2017; Gong and Xie, 2020). It is also linked to the plastic material itself, as additives and plasticizers are incorporated during the manufacturing process.(Wang et al., 2021a). Several studies have shown that weathered or partially aged MPs may have more hazardous impacts than pristine plastics (Arp et al., 2021; Liu et al., 2020). The dissemination of MP pollution predominantly originates in urban areas (Osterlund et al., 2023; Dhivert et al., 2024). It is conveyed through various components of urban hydrosystems, either through combined systems with wastewater treatment plant effluents and combined storm overflow or from separated systems, typically from stormwater management infrastructure (Wang et al., 2022). Therefore, understanding the behaviors of MPs within these hydrosystems is crucial for effective research and management.

MP degradation can affect the physicochemical characteristics of particles. Particle aging can affect the transport characteristics of MPs in water and their interactions with other contaminants and microorganisms (Duan et al., 2021). In the context of MP transport, the presence of oxidative bonds may generate more homo- and heteroaggregation with other pollutants and biofouling, drastically changing their transport mechanisms and paths (Sutherland et al., 2023). Furthermore, the formation of carboxyl groups reduces the surface hydrophobicity, thereby increasing the adhesion of other pollutants (Hanun et al., 2021). This implies a potential role as pollutant-bearing phases (Cui et al., 2024; Li et al., 2024). Some studies are interested in the adsorption of contaminants on weathered plastic particles, with metals being easily adsorbed (Sun et al., 2020), while the adsorption of organic pollutants is much debated, depending on the type of pollutant (Hüffer et al., 2018; Liu et al., 2019; Bhagat et al., 2022).

Today, the use of artificially aged particles is necessary for accurately simulating the environmental aging of microplastics (MPs) in natural conditions and for better understanding the key degradation mechanisms involved. From manufacturing to dissemination, MPs undergo many types of biotic and abiotic degradation, with the major abiotic phenomenon being photo-oxidation followed by mechanical and thermal degradation (Sun et al., 2020). Photo-oxidation degradation is the most efficient among

abiotic mechanisms and follows a three- phase mechanism, namely, initiation, propagation, and termination (Sun et al., 2020). In the initiation phase, carbon bonds absorb photons that generate free radicals. Throughout the propagation step, the interaction between radicals and oxygen leads to the formation of hydroperoxyl. Finally, in the termination phase, bonds are transformed into carboxylic acids, ketones, or hydroxyl end groups via a sequence of Norrish - type reactions (Zhang et al., 2023). In addition, for biotic pathways, MP biodegradation involves MP fragmentation and decomposition into degradation products of smaller molar weights, mainly through the bioconversion of carbon chains, which represent nutrient sources for microorganisms. Moreover, biofilms can settle on MP surfaces and increase MP degradation rates (Oberbeckmann et al., 2015; Zhang et al., 2023). These combined degradation phenomena cause specific chemical changes in MPs. Under abiotic degradation, chemical alterations result in the formation of oxygen bonds, such as carbonyl groups (including primarily ketones and secondarily esters and aldehydes), ether groups, and hydroxyl groups (Fernando et al., 2007; Gulmine et al., 2003; Hakkarainen and Albertsson, 2004). Conversely, in specific biotic degradation environments, oxygen-related changes suggest a higher formation of ester groups than in an abiotic environment, as shown by Albertsson et al. (1987). The presence of nitrogen in the atmosphere and urban water sources may lead to the generation of nitrogen–oxygen bonds in such biotic environments, and a notable concentration of alkene bonds can be observed. Indeed, Peixoto et al. (2022) highlighted the presence of nitrogen-oxygen and alkene bonds in the FTIR spectra of PE films degraded solely by micro-organism. Those functionalities are directly caused by the biodegradation of specific microorganisms (Ogihara, 1963; Hakkarainen and Albertsson, 2004; Peixoto et al., 2022). Methyl (CH_3) groups are associated with macrochain fragmentation induced by both biotic and abiotic degradation processes as shown explicitly by Albertsson et al. (1987) with the rise in the double bond (C=C) as a function of the weight of PE converted to CO_2 during biodegradation. In conclusion, each created chemical functionality can be attributed to degradation occurring in one or both environments, i.e., abiotic or biotic. In some cases, the attributes of the degradation pathway are defined however, usually, only the degradation environment can be confirmed.

As the resulting chemical changes can be attributed to degradation pathways, a better understanding of all the environmental stresses generating these changes is required to improve laboratory aging protocols (Sun et al., 2020; Zhang et al., 2023). Wang et al. (2021c) proposed an interesting comparison of laboratory and natural aging processes on polyethylene (PE) films. They showed that ultraviolet (UV) irradiation is the main factor responsible for the degradation of PE films, formation of cracks, and formation of oxygen functional groups on their surface. Burrows et al. (2024) looked at the differences in carbonyl index and showed that there is no difference between the use of natural and artificial UV degradation. However, there are contradictions regarding the type of degradation. Kalogerakis et al. (2017) showed that the chemical degradation of films is caused by UV radiation and that mechanical stress causes fragmentation in the second stage. Wang et al. (2021c) indicated that chemical oxidation generally occurs after physical changes to films. Sorasan et al. (2022) completed an analysis proposed by other studies that indicated UV irradiations fragment MPs into nanoplastics (NP). In particular, this result is consistent with an initial mechanical degradation that fragments debris into MPs followed by a photochemical reaction that fragments MPs into NPs. To address this issue, researchers have developed multiple protocols for manufacturing artificially aged plastics. Sun et al. (2020) provided a comprehensive review of MP abiotic lab-scale aging protocols, encompassing photo-oxidation coupled with mechanical abrasion or thermal degradation (Jelle and Nilsen, 2011; Song et al., 2017; Wang et al., 2021c). Only the work by Hsu et al. (2024) focused on the degradation of several types of polymer with weathered and digestion-degraded environments to provide an initial database of polymers degraded. All relevant information about the collected aging protocols is summarized in Table 1. These studies explored laboratory-controlled photo-oxidation aging protocols for plastic objects of various shapes and sizes. They range from hundreds of nanometers in size to plates of several millimeters. Photo-oxidation was performed either with natural sun exposure (Brandon et al., 2016; Kalogerakis et al., 2017; Wang et al., 2021c; Moreira et al., 2021) or for the majority of the studies with artificial UV. Exposure time and light power considerably vary, with the majority of the light emitting UV, resulting in a light intensity of a decade of watts per square meter. Finally, although the majority of the procedures are conducted dry, some protocols perform UV aging by immersing plastic samples in water. To the best of our

knowledge, a single study compared artificial aging to environmentally aged (Brandon et al., 2016). They showed that within the marine environment, Fourier transform infrared (FTIR) spectroscopy is an effective tool for assessing MP aging, although comparing it with aging under laboratory-controlled conditions presents significant challenges.

In this study, our analysis will be solely focused on the polymer type PE, which serves as the reference material in our research. This type of polymer is one of the most abundant polymers found in nature (Erni-Cassola et al., 2019), and its ubiquitous presence is primarily due to its use in single-use plastic (Chen et al. 2021). To address the growing concerns regarding the behavior of environmentally aged MPs in urban hydrosystems, there is a need to supply researchers with representative aged plastics for use in laboratory studies. To the extent of our knowledge, the present work addresses a gap in the scientific literature in several key aspects. Firstly, no statistical analysis on MPs degradation in urban hydrosystems has been conducted so far, highlighting a significant lack of quantitative data on the degradation processes of MPs in urban environments. Given the lack of degradation comparison between in-situ samples and samples from laboratory aging experiments, the first objective is to identify the representativeness and limitations of a protocol using accelerated UV photo-oxidation degradation. This involves comparing a large number of environmentally aged PE particles FTIR spectra with those subjected to a photo-oxidation degradation protocol in a controlled environment, as well as with those of common consumer materials before or after use. The second objective of this study is to identify the degradation intensities, environments, and preferred pathways across several matrices, including sediments, suspended solids, and stormwater, in a heavily anthropized urban stormwater detention basin.

	Light Wavelength	Exposure time	Light power	Polymers	Object type	Main Dimension	Ageing method	Additional Stresses
Jelle and Niksen (2011)	UVA or B	0-266 days	2.8-28 W/m²	PE,PP	Plates	15mm	Dry	-
Gardette et al. (2013)	300 nm	0-12 days	-	PE	Films	90-105µm	Dry	-
Lambert and Wagner (2016)	320-420nm	0-112 days	-	PE, PS, PLA, PP, PET	Plates	10mm	Wet	-
Brandon et al. (2016)	Sunlight	0-1080 days	-	PE,PS	Pellets	≥2mm	Dry or Wet	-
Song et al. (2017)	UVA or B or C	0-360 days	0.04-11 W/m²	PE,PP, EPS	Pellets	≥2mm	Dry	Abrasion
Kalogerakis et al. (2017)	Sunlight	0-180 days	-	PE	Fragments	100-700 µm	Dry	-
Cai et al. (2018)	340 nm	0-90 days	-	PE,PP,PS	Pellets	≥2mm	Dry or Wet	-
Da Costa et al. (2018)	254 nm	0-56 days	4 W/m²	PE	Pellets	≥2mm	Dry or Wet	-
Hüffer et al. (2018)	254 nm	4 days	30 W	PS	Particles	125-250 µm	Wet	Acid
Liu et al. (2019)	254nm	0-4 days	30 W	PS,PVC	Particles	75 µm	Dry	Acid
Zhu et al. (2020)	295-2500nm	0-150 days	682.5 W/m²	PS	Particles	≥0.22µm	Wet	Abrasion
Luo et al. (2020)	300-400nm	0-56 days	1200 W/m²	PE	Particles	≤150 µm	Dry	-
Lin et al. (2020)	254nm	90 days	1 W/m²	PE,PP,PS,PVC	Particles	≤250 µm	Dry	-
Wang et al. (2021c)	254nm or Sunlight	15 days	1 W/m²	PE	Films	6-15 µm	Dry or Wet	Acid + Abrasion
Moreira et al. (2021)	340nm or Sunlight	14-120 days	0.8 W/m²	PE	Films	17 µm	Dry	-
Bhagat et al. (2022)	254nm	4 hours	193.9 W/m²	PE	Plates	1cm	Dry	Acid
Sorasan et al. (2022)	280-400 nm	360 hours	1060 W/m²	PE,PP,EPS	Particles	1-5mm	Dry	-
Huang et al. (2023)	365nm	144 hours	200 W/cm²	PS, PLA	Particles	100 µm	Dry	-
Hsu et al. (2024)	300-830 nm	16 weeks	-	PE,PP,PS,PET, ABS	Pellets	3mm	Wet	Abrasion + Digestion
Burrows et al. (2024)	UVA (340 nm) Xenon-arc lamps (340 nm) Sunlight	168 hours 7 days 14 days	0.68 W/m²	PE, PP, PS	Nurdles	<5mm	Dry	-

The main dimension for films is the thickness and the biggest dimension for all others object types. UV-A (400-315 nm), UV-B (315-280 nm) and UV-C (280-100 nm)

Table 1: Summary of plastic object-aging and weathering photo-oxidation protocols with their intrinsic characteristics and parameters

2. Materials and Methods

2.1. Environmentally Aged MPs samples

In situ environmentally aged MPs samples were collected in a detention basin called Django Reinhardt located in the eastern part of Lyon, Chassieu, France. This basin stores stormwater from several urban catchment areas and traps micropollutants to prevent their release into the natural environment (Lipeme Kouyi et al., 2018). Several samples were collected and analyzed, including sediments accumulated in the basin, stormwater collected at the basin entrance, and suspended solids from a gully pot upstream of the basin entrance. Sediment samples were collected on April 6, 2022, by hand using a stainless steel shovel in the form of a composite sample (Figure 1(a)). Stormwater samples were collected during two rain events June 3, 2023, and October 18, 2023. The rainfall on June 3 was characterized by a basin-inlet average discharge of 0.49 $m^3 \cdot s^{-1}$, while that ~~of~~ on October 18 equaled 0.33 $m^3 \cdot s^{-1}$ (Figure 1(b)). The data from the two rainfall events were coupled to study PE spectral lengths of PE. These runoff waters were. Runoff water was collected from the basin inlet by an automatic sampler. Finally, suspended solids were collected with a pole during another rainfall event on November 9, 2023 (Figure 1(c)).

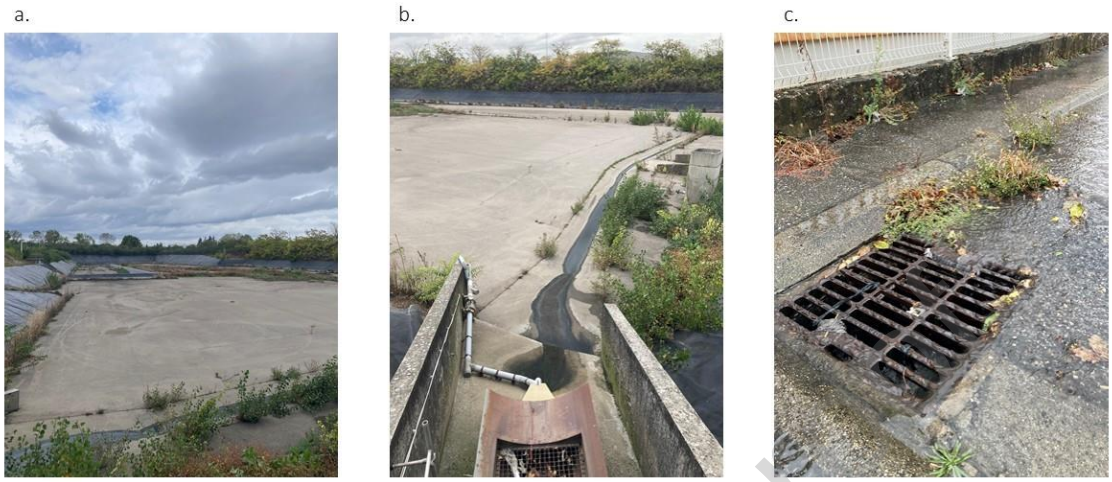

Figure 1: (a) Dry Django Reinhardt basin where sediment samples were collected. (b) Entrance to basin with an automatic sampler inside to collect stormwater samples. (c) Gully pot upstream of detention basin where trapped suspended solids were sampled.

The extraction protocol for MP identification was essentially the same for all samples. This protocol includes densimetric separation using a solution of sodium iodide of density 1.67 $g \cdot cm^{-3}$ to segregate organic and mineral elements (Nakajima et al., 2019). Then, an organic degradation step was done with hydrogen peroxide at 30%. Finally, the filters were analyzed by micro-FTIR spectroscopy, and all detected MPs (25 µm ≤ MPs ≤ 500 µm) were identified using siMPle software (Primpke et al., 2018). SiMPle software allows qualitative detection of the polymer type in all detected particles. For more details on this protocol, please refer to Iannuzzi et al. (2024). However, the order of steps slightly differed between the three sample matrices. As the stormwater and suspended solid samples contained a high organic matter content, it was necessary to perform the oxidation of the organic matter first and repeatedly, as long as it was still visible. PE particles were easily isolated by applying a filter to the databases to retrieve only the PE particle spectra. The MP concentrations measured in these samples were very high compared with the literature. For the sediment samples, we found approximately 571,178 $MPs \cdot kg^{-1}$ of dry sediment (dw) and approximately 115,451 $PE \cdot kg^{-1}$ dw, which corresponds to 20.2% of the total MP particles.

For the stormwater samples, the first rainfall recorded a total of 2,272 MPs·L^{-1} including 316 PE·L^{-1} and the second rainfall recorded a total concentration of 3,746 MPs·L^{-1} including 481 PE·L^{-1}, representing a total PE contribution of 13%. Finally, for the gully pot suspended solid samples, the concentration of MPs was 980,000 MPs·L^{-1} including 281,428 PE·L^{-1} representing a total PE contribution of 29%. A wide array of PE particle spectra from diverse matrices was employed in this study, namely, sediments (n = 228), stormwater (n = 685), and suspended solids (n = 197).

2.2. Common consumer materials selection

An analysis of common consumer materials was conducted to assess their degradation state following normal usage and to establish a link between the *in situ* environmentally aged MPs and the degradation environment. This was done to control that degradation was primarily driven by the environment after disposal, rather than their lifespan. Six different plastic objects made of LDPE, commonly used in everyday life and industry, were selected (Table S1). Two of these objects were compared before and after use to assess degradation potentially linked to single use. For all objects, three FTIR spectra were taken and averaged to account for the overall degradation state.

2.3. Artificially aged films

Nonadditivated low-density PE (LDPE) Lupolen 2420 F was used as the material to process films of a constant thickness of 200 µm through molten-state by extrusion. This commercial PE is used as a consumer product in agricultural films or food packaging. To ensure effective processing of the film, several thermomechanical cycles were conducted before extrusion. Using virgin films for photo-oxidation aging offers the advantage of concentrating the oxidative chemical functional groups formed on the surface for mass analysis and enables rapid observation of the aging kinetics.

Burrows et al. (2024) highlighted that despite emitting at different wavelengths, the degradation state of plastic films exhibits a similar level for the same exposure intensity power. Films were thus exposed to intense UV-A exposure of increasing duration, using a UWAVE ULINE-365 lamp, set to an intensity of 65%, a wavelength of 365 nm, a resulting power of 55705 W/m^2 with temperatures reaching 80°C due to lamp heating. This

irradiation value exceeds the 482 W/m^2 annual solar irradiation in the City of Lyon, France (European Commission, 2022). On average, 1 h of bench UV exposure is equivalent to 115 h of cumulative sun exposure. To ensure uniform exposure, all films were centrally positioned under the lamp and flipped upside down every 8 h. These objects underwent a maximum of 48 h of exposure (equivalent to around 1.2 years of 12 h a day of sun exposure in Lyon). Such intense exposure was employed to accelerate the aging process of plastics. Moreover, emphasizing that the majority of plastic photo-oxidation occurs under dry conditions, the films were also deliberately degraded herein within a dry matrix. For each artificially aged film, the FTIR spectra were measured three times at random locations and showed no significant variations. The resulting spectra were then averaged.

2.4. FTIR

For the artificially aged films, a Nicolet iS10 FTIR machine coupled with OMNIC software was used for FTIR spectral analysis in attenuated total reflectance (ATR) mode using diamond in the range of 500–4000 cm^{-1}. For common consumer materials, an analysis in ATR was also performed with a PerkinElmer Spotlight 400 FTIR Spectrum 3 coupled with SpectrumIMAGE software©. The analysis was in the range 500-4000 cm^{-1}. Concerning environmentally aged MPs, the same FTIR was used for a micro-FTIR spectral analysis with the imaging system. The analysis was in transmittance mode between the range 1250-3650 cm^{-1}. Based on the bonds and groups identified by PE degradation, the interpretable peaks and bands in the FTIR spectra corresponding to specific groups are listed in Table 2. The oxidative bonds are hydroxyl groups (3000–3500 cm^{-1}), carbonyls (1670–1800 cm^{-1}), and ethers (1000–1310 cm^{-1}) (Albertsson et al., 1987; Lacoste and Carlsson, 1992; Socrates, 2004; Pavia et al., 2014; Brandon et al., 2016; Sandt et al., 2021). For nitrogen-linked bonds, the range of carbon–nitrogen bonds linked to amine groups is 1020–1280 cm^{-1}. However, their overlap with the ether region makes their identification challenging (Pavia et al., 2014). The range of the oxygen–nitrogen bond equals 1500–1550 cm^{-1} centered at 1520 cm^{-1} does not interfere with another oxygenated region (Peixoto et al., 2022; Ogihara, 1963). Finally, for carbon–carbon bonds, two spectral signatures can be easily detected in all spectra: CH_3 groups (1350–1400 cm^{-1}) and alkene bonds (1600–1670 cm^{-1}).

Similarly to the specified area under the band carbonyl index (SAUB CI = area under the band 1850–1650 cm^{-1}/1500–1420cm^{-1}) as proposed by Almond et al. (2020), bond indices were calculated by dividing the specified area under the band range, as defined in Table 2, by the area of the reference peak. In this work, the reference peak is defined at 1463 cm^{-1}, which corresponds to the bending deformation of CH_2, and the area delineated by Almond et al. (2020) (1500–1420 cm^{-1}), which is characteristic of PE and exhibits minimal variation with weathering (Socrates, 2004). Finally, all FTIR baselines were corrected using the method recommended by Shen et al. (2018).

Group or bond	Chemical formula	Band range (cm^{-1})	Main peak (cm^{-1})	Deg. pathway
Hydroxyl	R—OH	3000—3500	3380	Abiotic
Carbonyl	R—C(=O)—R′	1670—1800	1715*	Abiotic
Alkene	R—C=C—R′	1600—1670	1650	Biotic
Nitrogen–Oxygen	R—N—O—R′	1500—1550	1520	Biotic
Methyl	R—CH_3	1350—1400	1375	Both
Ether	R—O—R′	1000—1310	1150	Abiotic

**1715 cm−1 is associated with ketones, and the secondary peaks at 1735 and 1775 cm−1 are related to esters and peroxides.*

Table 2: Characteristic degradation groups and bonds with their respective chemical formulas, band ranges, and main peaks of their FTIR spectral signatures

2.5. Solid-state ^{13}C NMR

High-resolution nuclear magnetic resonance (NMR) spectra of pristine films and 24-h UV-aged films were recorded to determine the presence or absence of functional groups resulting from photo-oxidation degradation. This technique can serve as a validation tool for FTIR spectroscopy analysis and evaluation of internal structural changes caused by photo-oxidation. The NMR spectra were collected using a Bruker AVANCE 400 MHz spectrometer operating at 100.6 MHz for ^{13}C and equipped with a 4 mm 15N-31P/1H-19F solid probe using magic angle spinning (MAS) and a pulse sequence with cross polarization (CP) with a contact time of 500 μs. The samples were placed in a zirconium rotor rotated at 10 kHz. A total of 4000 scans were conducted for each spectrum with an acquisition time of 25 ms and a delay between each pulse of 10 s. Chemical shifts were measured in agreement

with the glycine carbonyl signal at 176.03 ppm and the adamantane signal at 38.48 ppm. The analysis presented here outlines the presence of specific chemical functionalities, as detailed below. However, it does not include information about their concentrations. Note that conducting this analysis of environmentally aged was not possible due to the limited available mass of them.

Coupled with the FTIR spectra and based on the literature on PE photodegradation, several groups and bonds were expected in the 24-h-UV aged NMR spectrum (Table 3). (Bovey et al., 1988; Han et al., 1999; Assink et al., 2000; Banfi and Patiny, 2008).

Group or bond	Chemical formula	Expected peaks (ppm)
Ketone	R—C(=O)—R′	210
Aldehyde	R—C(=O)—H	205
Carboxylic Acid	R—C(=O)—OH	178
Ester	R—C(=O)—O—R′	170
Carbonate ester	R—O—C(=O)—O—R′	155
Hydroxyl	R—OH	71.9
Ether	R—O—R′	72.0
α-Carbon of a ketone	R—**C**—C(=O)—R′	42.5
β-Carbon of a ketone	R—**C**—C—C(=O)—R′	24.0
Methyl group	R—CH_3	14.0

Table 3: Characteristic degradation groups and bonds with their respective chemical formulas and expected peaks of their ^{13}C NMR spectral signatures

3. Results and Discussion

3.1. Environmentally aged MPs analysis

Figure 2 shows the average median PE spectra among all identified PEs in environmental samples of stormwater, urban sediments, and suspended particles. Six groups and bonds were easily identified using FTIR spectroscopy (Table 2). Excluding the ether bond (1000–1310 cm^{-1}), which is out of the acquisition range for the spectrometer used for MP analysis, it can be observed that all five regions of interest present non-negligible bond indices

(normalized absorbance intensity on a reference peak) for all three in situ matrices. Nitrogen–oxygen and alkene bonds present non-negligible bond indices, revealing partial biodegradation of the polymer according to the conclusions of Albertsson et al. (1987) and Peixoto et al. (2022). Similarly, carbonyl and hydroxyl bond indices are thought to reveal abiotic degradation (Gardette et al., 2013; Cai et al., 2018).

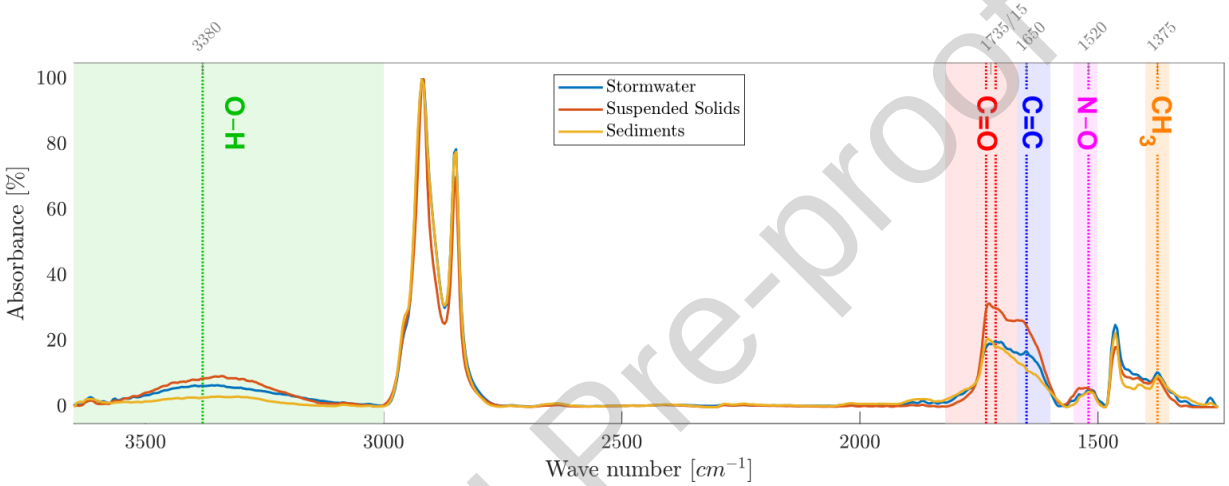

Figure 2: Median FTIR spectra of in-situ environmentally aged PE particles found in stormwater, sediments, and suspended solids matrices.

Figure 3 shows the relative abundances of all degradation chemical groups and bonds with the 5th, 25th, 50th, 75th, and 95th percentiles as boxplots for stormwater, suspended solids, and basin sediments. The absorbance of the hydroxyl bond (O–H) is higher for suspended solids and stormwater, particularly the 95th percentile, which exceeds 20%, suggesting a higher degree of hydrolysis degradation in those matrices (Brandon et al., 2016; Wang et al., 2021c). Notably, samples collected from water matrices tended to exhibit a higher prevalence of hydroxyl bonds. For the carbonyl (C=O) and alkene (C=C) groups, there is no significant difference in the order of magnitude between stormwater and sediments (30% and 18%, respectively), but a higher value is observed for suspended solids (35% and 30%, respectively). Finally, for the CH_3 group and nitrogen–oxygen bonds, all matrices have equivalent values of approximately 8% and 10%, respectively. In conclusion, no significant difference in distribution ranges was observed between the three samples.

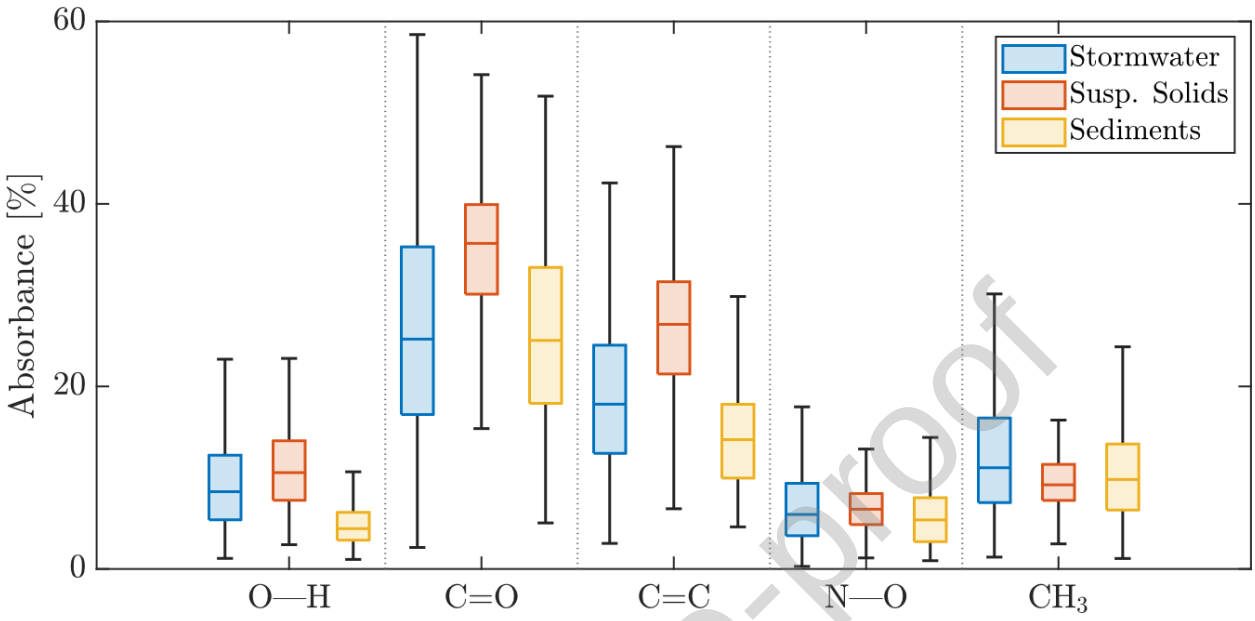

Figure 3: Boxplot panel of intensity of bond indices in FTIR spectra for all collected environmentally aged.

Moreover, the median SAUB CIs for the environmentally aged MPs were reported to be 2.51, 4.36, and 3.21, respectively, for stormwater, suspended solid, and sediment MP matrices. Therefore, the median spectra and SAUB CI confirm that the environmentally aged particles are in an advanced degradation state. This differs from the literature data on in situ stormwater-collected PE by Ramirez-Alvarez et al. (2020), who presented the spectrum of a typical PE found in wastewater treatment plant effluent. Their spectrum analysis indicated the absence of characteristic degradation bonds, especially carbonyl bonds. However, an ether bond can be found around 1000 cm^{-1}. Wang et al. (2021b) investigated particles in the surface water of a river and observed a PE spectrum with minimal degradation because no weathered bonds were observed. Other research studies have demonstrated typical aged PE particles collected in urban rivers with various clear peaks for hydroxyl, carbonyl, and alkene bonds and a large ether band (Zhang et al., 2022; Hossain et al., 2023). Our spectral analysis confirmed that the environmentally aged PE particles were largely aged compared with those reported in other studies, although our study lacks the ether bond estimation required to fully assess degradation.

When more carefully examining the carbonyl bonds, distinct spectral signatures emerged among the environmentally aged MPs spectra. Figure 4(a) illustrates these signatures from three different MP sample spectra of the stormwater matrix, each focused on the carbonyl band. The blue spectrum represents a predominant carbonyl group associated with the ester peak (1735 cm^{-1}), the red spectrum exhibits a major carbonyl group associated with the ketone peak (1715 cm^{-1}), and the purple line exhibits both peaks of similar magnitude.

Studies by Albertsson et al. (1987) and Karlsson and Albertsson (2002) demonstrated that PE degradation in biotic environments has a blue spectrum with a major ester peak, whereas PE degradation in abiotic environments has a red spectrum with a dominant ketone peak. The purple spectrum suggests a degradation process influenced by a mix of both environments. The primary degradation environment of our in situ environmentally aged samples (whether biotic or abiotic) can be determined. Figure 4(b) shows the relative numbers of each sample type across the three matrices (stormwater, suspended solids, and sediments). It appears that for 68.1% of the in situ stormwater-collected environmentally aged MPs, the main degradation environment is abiotic, while the opposite stands for sediment and suspended solid environmentally aged, with 57.6% and 64.8% of them having a biotic main degradation environment, respectively.

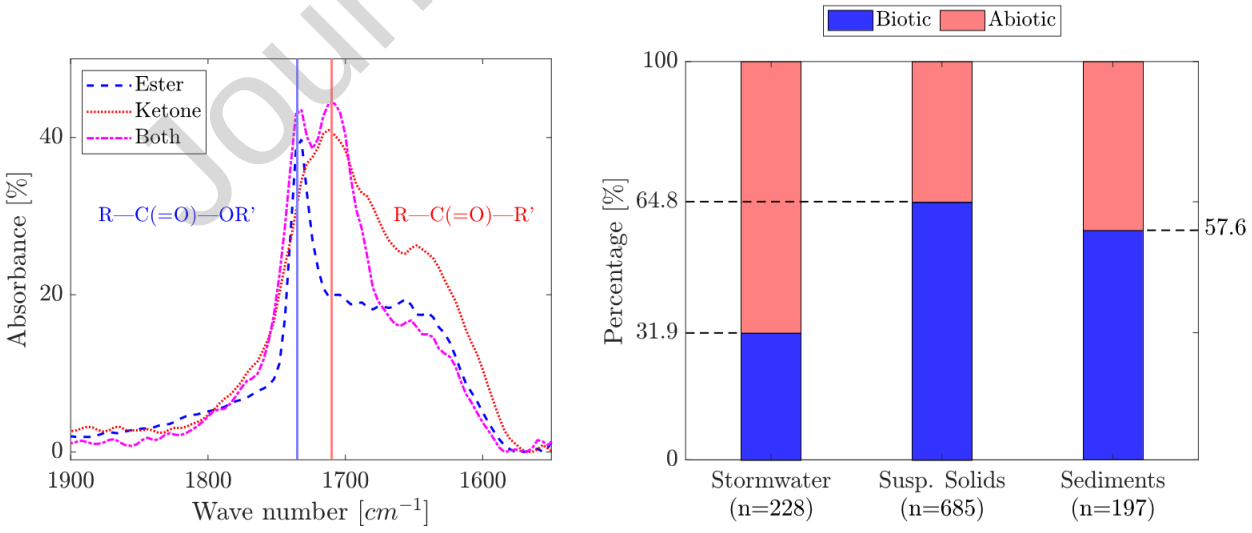

Figure 4: (a) Three environmentally aged PE particles spectra from stormwater matrix around the carbonyl band displaying the three patterns and main peaks associated in the region. (b) Estimated distribution of

degradation environments for all three in situ environmentally aged MPs sample matrices based on the comparison of the carbonyl groups associated with ester and ketone peak absorbances.

3.2. Aging experiment analysis

Nonadditivated LDPE films were exposed to UV radiation for a maximum cumulative time of 48 h to generate rapid photo-oxidation corresponding to 1.2 years of natural photo-oxidation at the study site. Figure 5 shows the FTIR spectral evolution of the artificially aged films.

The formation of carbonyl, CH_3, and ether groups was observed in the aged spectra. Due to the abiotic degradation method, no markers of biotic degradation were found (N–O and C=C). In addition, no hydroxyl group spectral signature is observed during UV exposure. Sandt et al. (2021) and Gardette et al. (2013) identified several peaks in the carbonyl band. The carbonyl group associated with the ketone peak (1715 cm^{-1}) dominates, followed by the carbonyl group associated with the ester peak (1735 cm^{-1}), and the carbonyl group associated with the peroxide peak (1775 cm^{-1}) is only visible for high-level degradation. This trend is expected in our abiotic aging environment.

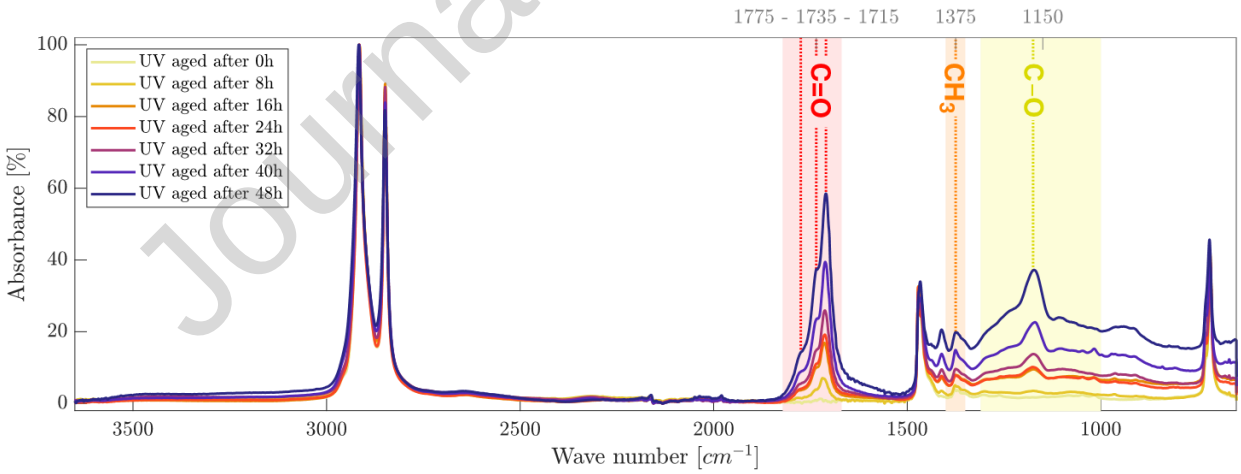

Figure 5: UV-aged FTIR spectra of nonadditivated LDPE artificially aged films. The aging duration ranged from 0 to 48 h, with an increment of 8 h.

Figure 6 shows the SAUB bond indices of CH_3, ether, and carbonyl as functions of UV-light exposure time for the UV-aged films. The carbonyl and ether indices increased at the same rate, indicating similar concentrations for both oxidative functions on the artificially

aged film surface, while a much slower increase in CH_3 occurred. The same kinetic tendency for the carbonyl index was observed in an aging study by Gardette et al. (2013). Almond et al. (2020) and Bhagat et al. (2022) reviewed studies that collected the classical carbonyl index (=1714/1463 cm^{-1}) range of aged PE, highlighting maximum values at 1.1 and 0.9, respectively. In our study, however, we observed a classical carbonyl index reaching up to 1.67 for artificially aged films, indicating that the aging process induces a considerable level of oxidative degradation. In addition, based on the FTIR spectra, the crystallinity of the material can be estimated using the 730 and 720 cm^{-1} peaks (Stark & Matuana, 2004; Colom et al., 2000; Zerbi et al., 1989). Crystallinity increases with exposure time, starting from 65% for unaged MPs and reaching 95% for the 48-h-UV-aged films. Indeed, the shortening of the polymer chains at high temperatures allows them to rearrange more easily into a structured organization, resulting in higher crystallinity values.

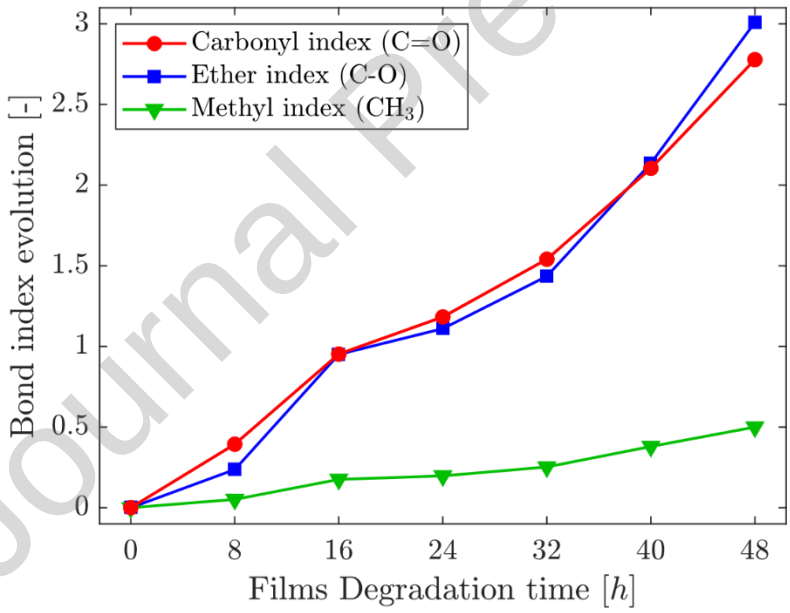

Figure 6: Time evolution of SAUB bond indices (carbonyl in red, ether in blue, and methyl in green) for artificially UV-aged films.

For a better and more precise understanding of the chemical changes induced by UV-light exposure of the compounds, solid-state CP MAS ^{1}H–^{13}C NMR analysis was performed for pristine and 24-h UV-exposed films. Figure 7 shows the spectral signature, i.e., the chemical displacement δ in parts per million (ppm) as a function of the intensity in

percentage of the maximum intensity. Based on the several peaks that can denote the photo-oxidation degradation of PE presented in Table 3, which were already observed using the FTIR spectra, ketone (207.8 ppm), ester (172.2 ppm), and CH_3 (13.8 ppm) were clearly identified. Two other peaks also demonstrate the presence of ketone in bulk, namely, α-carbon and β-carbon linked to ketone (42.5 and 23.8 ppm, respectively). Other chemical groups that are highly difficult to identify in FTIR spectra can be observed using NMR analysis, such as carboxylic acid (179.4 ppm) and carbonate ester (156.0 ppm). These groups enable us to further characterize the oxidation state of artificially aged PE films. Finally, for the peak at 71.9 ppm, two attributions can be made according to the literature: a secondary hydroxyl bond (Bovey et al., 1988) or an ether bond (Banfi and Patiny, 2008). Because no hydroxyl groups were identified in the FTIR spectra, it is more likely that this peak corresponds to ether groups.

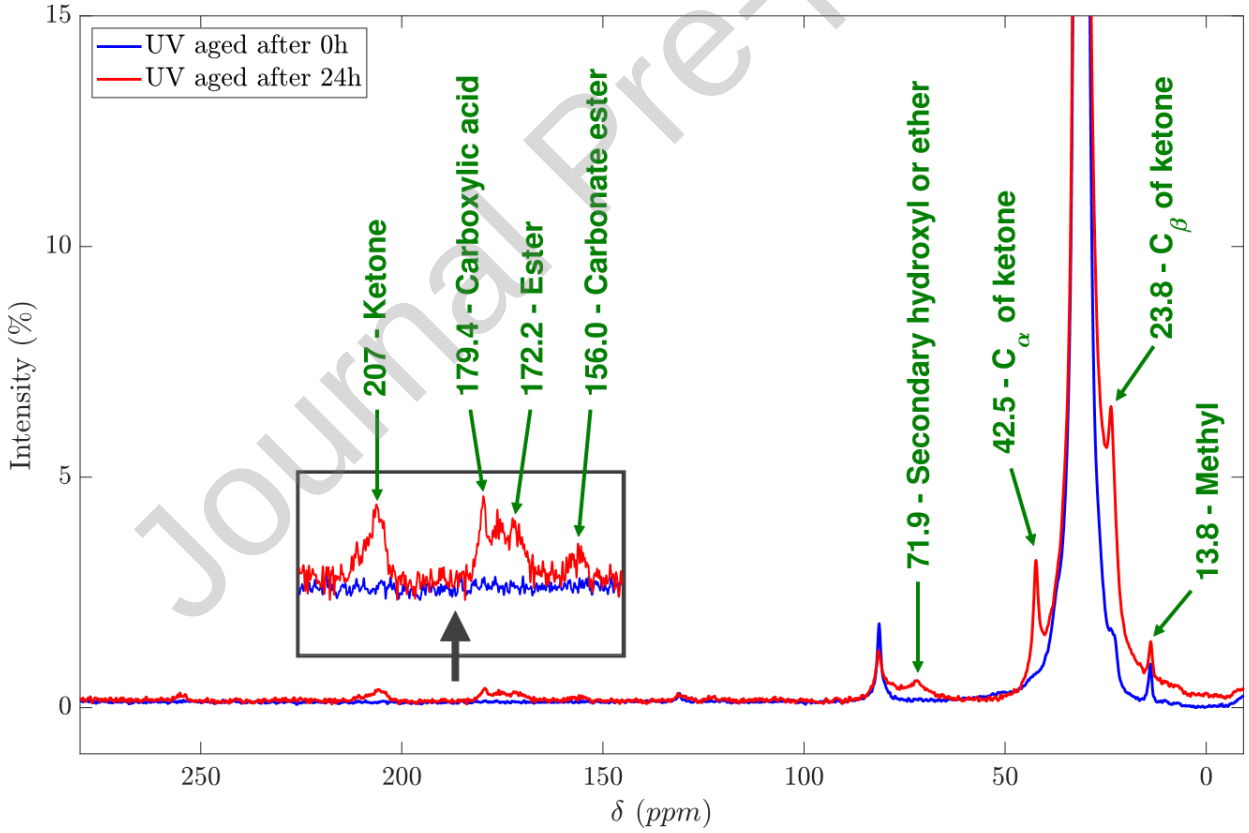

Figure 7: Solid-state ^{13}C NMR spectra of pristine and 24-h-UV aged films

The NMR spectra confirmed the degradation-induced chemical changes observed by FTIR. Quantitative NMR analysis is only possible after a considerable amount of time. Due to this limitation, an evolution of the concentration of aged chemical groups as a function of exposure time was not obtained. The coupling of NMR spectra with FTIR spectroscopy allowed us to confirm the chemical changes induced by degradation, as observed. However, quantitative NMR analysis is time-consuming. Consequently, the evolution of the aged chemical groups over exposure time in NMR data could not be tracked.

3.3. Comparative analysis of spectral data from environmentally and artificially aged materials

A direct comparison between the median spectra of environmentally aged and UV-aged films is shown in Figure 8(a), (b), and (c) for stormwater, suspended solids, and sediments, respectively. These figures illustrate the median environmentally aged MPs FTIR spectra in green and all FTIR spectra from UV-aged films in dashed-dotted lines, except for the closest match represented by a thicker solid line.

The closest match was determined by comparing the general spectral shape and, more specifically, the carbonyl absorbance values. To improve clarity, the wavelengths from 2650 to 1950 cm^{-1} with no degradation signature were removed.

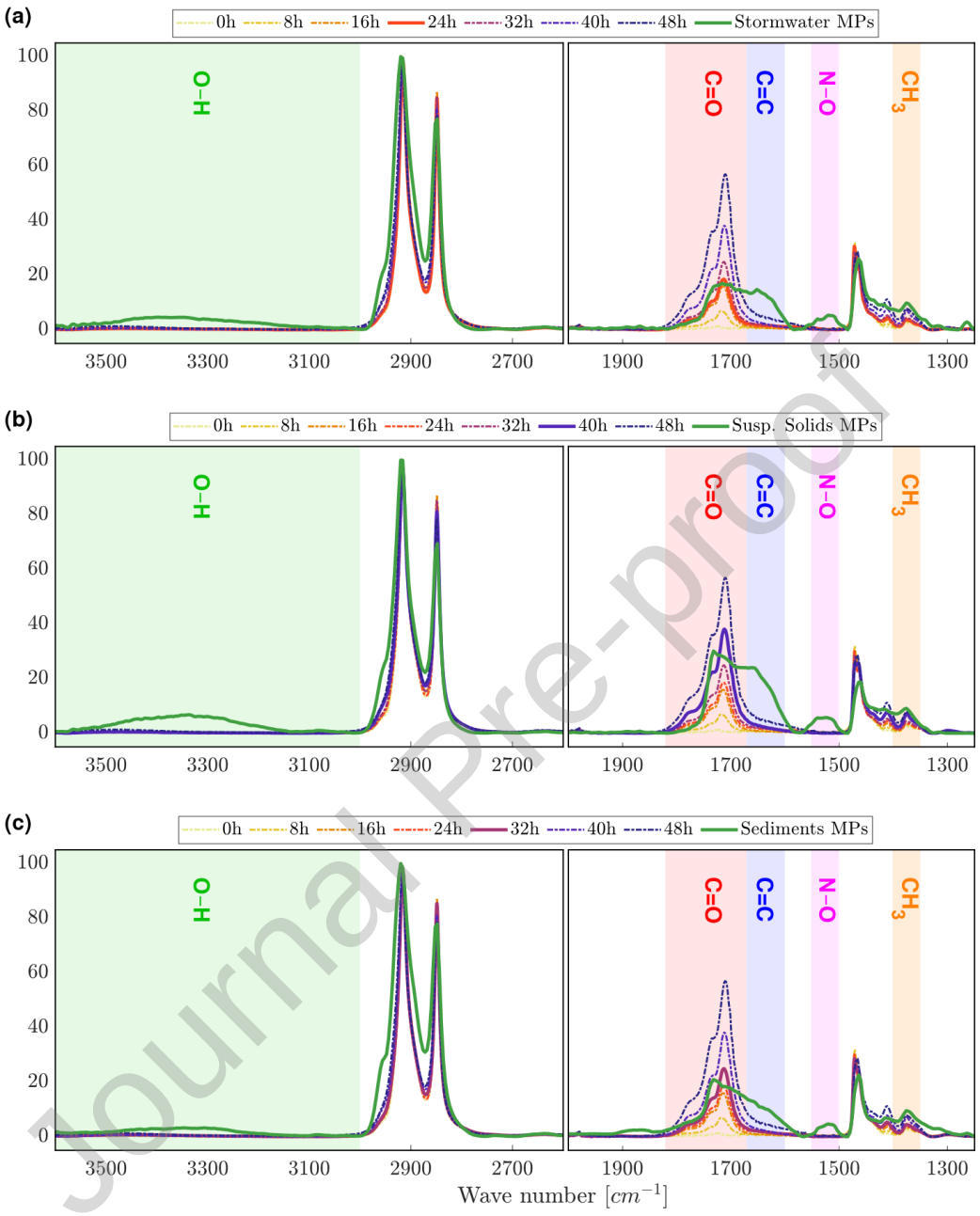

Figure 8: Comparison of FTIR spectra of artificially aged films and environmentally aged in stormwater (a), suspended solids (b), and sediment samples (c). All film spectra are plotted in dash-dot line, except for the closest environmentally aged sample, which is plotted as a thick plain line. All plots were cut in the 2650–1950 cm^{-1} area, resulting in no degradation signature.

Several observations can be made following the analysis of Figure 8.

(1) The spectrum of the 24-h-UV aged film resembled the median spectrum found in stormwater; for the median spectrum found in suspended solids in the gully pot, it is the 40-

h-UV aged film; the 32-h-UV aged film aligned closely with the median spectrum of sediments.

(2) The absence of hydroxyl (O–H) groups in the artificially aged films is noteworthy. This can be explained by UV exposure being conducted under dry conditions (with the particle nonimmersed in water), which impedes free radicals from reacting with water to form hydroxyls (Brandon et al., 2016; Wang et al., 2021c).

(3) Environmentally aged exhibit markers of both biotic and abiotic degradation, whereas UV-aged films exhibit only abiotic degradation (photo-oxidation), specifically, alkene (C=C) and nitrogen–oxygen bonds (N–O) are absent in UV-aged films because of the purely abiotic nature of the degradation process (Peixoto et al., 2022; Zhang et al., 2022; Hossain et al., 2023).

(4) Advanced stages of carbonyl functional degradation (C=O) are observed in all spectra. Nonetheless, the dominant peak of the carbonyl band, which corresponds to different chemical functional groups, varies between the two. In environmentally aged present in sediments and suspended solids, ester peaks are predominantly higher than those found in stormwater and UV-aged films. This discrepancy in our study can be attributed to the prevalence of a biotic environment over an abiotic environment in sediments and suspended solids (Figure 4(b)).

(5) For the UV-aged films, CH_3 groups were present in similar proportions to those observed in all in situ environmentally aged particles. UV-aged films exhibit significant ether (C–O–C) bonds (Figure 5), but due to the limited wavenumber range, such detection and comparison of their signatures with those of environmentally aged particles were not possible. To conclude, as shown in Figure 8(a), an excellent overlap occurs, except for the hydroxyl groups, especially in the carbonyl band. For the CH_3 peak, it is worth noting that microorganisms play a significant role in breaking down polymer chains and increasing the concentration of CH_3 groups (Albertsson et al., 1987). This accounts for the less precise overlap in that region. Overall, in qualitative terms, the artificial aging process aptly reflects abiotic degradation in the environment.

The spectral signature of the carbonyl band is one of the most widely recognized indicators of PE degradation in the scientific literature (Albertsson et al., 1987; Sandt et al.,

2021). As demonstrated in this study and in the literature, according to numerous authors, when biodegradation occurs on PE in a biotic environment, alkene formation is evident in the FTIR spectra. This chemical functional group exhibits a spectral signature at 1600–1670 cm^{-1}, very close to that of carbonyls, which complicates the use of integral criteria such as the SAUB CI (Almond et al., 2020).

To accurately assess the concentration of carbonyl groups, two separation methods were used. The first method involved reducing the range over which the SAUB CI was calculated (1670–1850 cm^{-1}) to minimize the influence of alkenes. The resulting values then adjust to {2.63, 3.28, 2.14} for stormwater, suspended solid, and sediment matrices, respectively. The CI values for stormwater and sediment matrices correspond to degradation in the range of 40–48 h for our artificially aged films, whereas the value for suspended solids greatly exceeds this value (Figure 6). The main drawback of this method is the difficulty in comparing the newly derived SAUB values to those from the literature. To address this issue, the second method uses spectral peak deconvolution, similar to that used by Gardette et al. (2013), to decompose the contribution of each bond and chemical functional group present in the carbonyl–alkene range (1565–1850 cm^{-1}). The number of spectra per matrix was considered sufficient for spectrum deconvolution. For each sample matrix, a preselected number of four peaks was selected based on visual observation. Subsequently, Gaussian fitting using a least-squares method was applied to each matrix's median spectrum, with all equation parameters (height, center position, and standard deviation) left free, while the maximum width of each peaks has been limited (Maddams and Parker, 1989). The spectral deconvolution of the stormwater, suspended solid, and sediment matrices is shown in Figure 9(a), (b), and (c), respectively. All solid lines correspond to the measured spectra of the corresponding matrix and the UV-aged film equivalent. Additionally, four independently fitted Gaussian curves corresponding to the peaks of carbonyl groups associated with (i) peroxide, (ii) ester, (iii) ketone, and (iv) alkene bonds are displayed as black dotted lines. Finally, the dashed-dotted lines correspond to the reconstructed spectra based on Gaussian fitting, with the orange line representing the reconstructed carbonyl peak excluding the peak associated with the alkene bond (i + ii + iii, excluding iv) and the yellow line representing the entire reconstruction (i + ii + iii + iv).

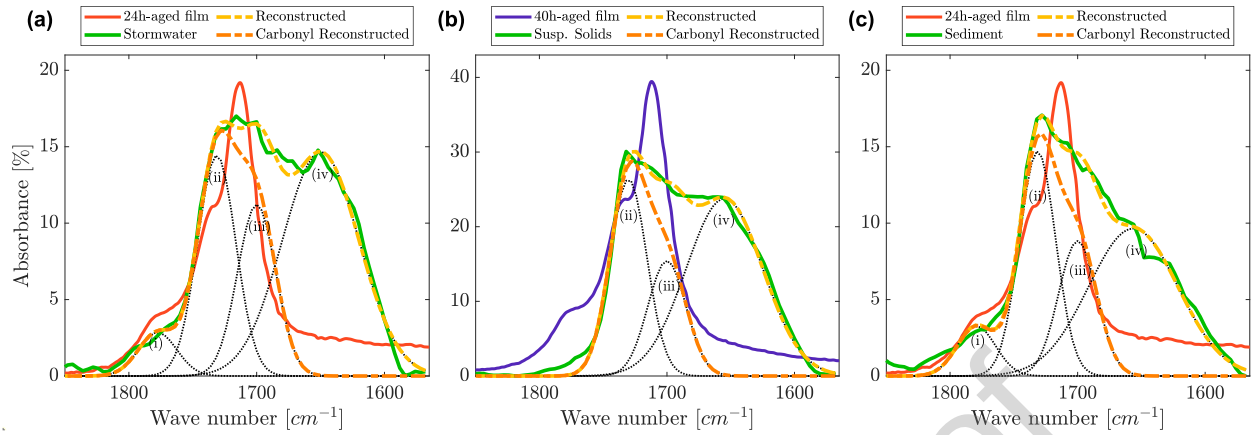

Figure 9: Spectral deconvolution of FTIR spectra around the carbonyl band (1565–1850 cm^{-1}) of median MP spectra of (a) stormwater, (b) suspended solid, and (c) sediment matrices. The closest artificially aged film matches are also shown for each matrix. Four independently fitted Gaussian curves corresponding to carbonyl groups associated with (i) peroxide, (ii) ester, (iii) ketone, and (iv) alkene bonds are displayed in the dotted line. Reconstructed spectra are plotted in dash-dot line.

Upon observation of the deconvoluted environmentally aged spectral signatures of suspended solid and sediments, it appears that the peak of carbonyl groups associated with ester exhibits higher absorbance than those associated with ketone for all matrices. Furthermore, it is noteworthy that the peroxide peak (i) is absent in the suspended solid matrix. Except for this absence, it can be observed that MPs in all matrices exhibit similar chemical changes, which can be explained by the presence of almost the same peaks in all matrices. A very close match of the environmentally aged spectral signature was achieved for every matrix based on the four Gaussian distributions. Spectral deconvolution enabled us to isolate these four distinct peaks corresponding to four chemical functional groups, thereby facilitating the separation of the alkene peak (iv) from the carbonyl bond.

For the second method, the SAUB CI was computed based on the reconstructed carbonyl peak, excluding the portion corresponding to the alkene peak from the deconvoluted spectra. The resulting values then adjust to {1.22, 2.26, 1.55} for the three matrices, which differ significantly from those calculated using the first method when considering the alkene peak based on the CI definition. These corrected CI values correspond to laboratory artificially aged film degradation over a range of 32–48 h (Figure 6), supporting the visual comparison shown in Figure 8. The different CI values are summarized in Table 4. Although

it may seem somewhat unconventional, this approach accounts for the influence of the alkene band and allows visual observations of the exposure time required to represent environmentally aged. Considering specific peaks and using spectral deconvolution ranges to compute the carbonyl index is important.

	Stormwater	Suspended Solids	Sediments
Standard definition	2.50	4.96	2.95
1st method	2.63	3.28	2.14
2nd method	1.22	2.26	1.55

Table 4: Comparison of SAUB carbonyl index values: standard definition of alkene influence, adapted range for CI (1st method), and reconstructed spectra via spectral deconvolution excluding the alkene peak (2nd method)

3.4. Investigating degradation processes and trends

Principal component analysis (PCA) was performed to evaluate the representativeness of the artificially aged films compared to the environmentally aged MPs and common consumer materials (Table S1, Figure S1). The dataset included the FTIR median spectra of the three environmentally aged MP matrices, the FTIR spectra of the common consumer materials (two before and six after use), and spectra of several artificially aged films (0, 24, 32, and 40 h). The PCA was performed on the four FTIR wavelengths corresponding to the chemical bonds of degradation: hydroxyl (3000–3500 cm^{-1}), carbonyl (1670–1800 cm^{-1}), alkene (1600–1670 cm^{-1}), and nitrogen–oxygen (1500–1550 cm^{-1}).

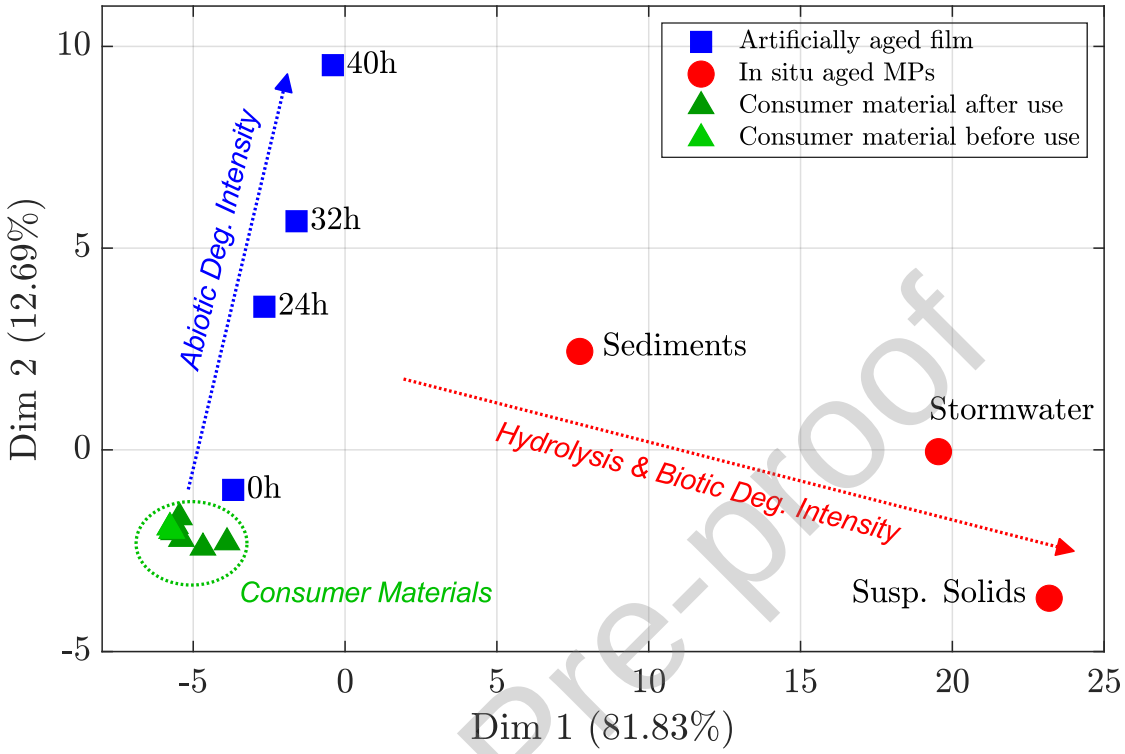

Figure 10: PCA of UV-aged PE artificially aged films, the common consumer materials (before or after use) and environmentally aged PE particles median FTIR spectra. PCA was performed at four wavelengths to evaluate the degradation of chemical bonds

Figure 10 shows the two principal dimensions in which the spectra are predominantly present, collectively explaining approximately 95% of the variables. The blue vector drawn in the figure represents the intensity of abiotic degradation in the carbonyl range. Notably, the reference spectra depicting the common consumer materials (before or after use) are all in the vicinity of the unweathered polymer (pristine film). All consumer materials are positioned distinctly at the bottom left of the graph, while the highly aged PE spectra (such as the 40-h-UV aged films) are located at the top left. Using a similar methodology, Da Costa et al. (2018) reported differences between the spectra of artificially aged particles and their initial counterparts. Conversely, the dimension orthogonal to the blue vector (the red one) highlights plastics aged in the urban environment displaying hydrolysis and biodegradation markers, in addition to abiotic degradation. The difference in degradation between MPs

found in sediments compared to those in stormwater and suspended solids can be explained by the higher relative absorbance of hydroxyl and alkene groups in the latter (Figure 2). These results confirm that humid conditions promote biotic processes. Through this axis decomposition, it can be observed that all three MP matrices exhibit intermediate degradation, consistent with the visual comparison illustrated in Figures 8 and 9. However, a non-negligible gap was observed between common consumer materials and UV-aged films with environmentally aged MPs for all matrices, suggesting only a partial representativeness of laboratory-aged objects. Furthermore, the comparison with common consumer materials suggests that the majority of the degradation likely occurs when plastic objects are discarded in the environment, as all these objects are close in condition to the pristine film (0 h-aged). This observation was to be expected, as most LDPE objects are manufactured to be single-use (Chen et al., 2021).

4. Conclusion

Through the integration of spectroscopic techniques and statistical analysis, a better understanding of the chemical changes induced by both environmental and artificial aging processes was achieved. This study provides valuable insights into the degradation of PE particles in urban hydrosystems. First, all environmentally aged of PE present high levels of abiotic and biotic degradation with the most of it occurring in the environment after its use. Still, degradation under biotic environments appears dominant for MPs in sediments and suspended solids, while degradation under abiotic environments is more pronounced for MPs collected in stormwater. Second, the artificial photo-oxidation aging protocol used in this study using intense UV radiation effectively simulates abiotic degradation similar to that observed in environmentally aged within a relatively short timeframe (less than 48 h). By combining visual observation, carbonyl indices, and PCA, the best agreement with in situ environmentally aged PE particles was achieved using non-additivated PE plastics aged over approximately 36 hours. This aging corresponds to a cumulative energy exposure density of 48.2 MJ/m^2, which is equivalent to slightly less than a year of natural UV oxidation at the study site.

Photo-oxidation degradation protocols under dry conditions do not effectively represent in situ environmental degradation in urban hydrosystems. Major improvements to aging protocols should involve significant humidity during UV exposure to artificially aged films or exposure conducted in water immersion to generate substantial hydroxyl formation, as already mentioned by Brandon et al. (2016) and Wang et al. (2021c). Furthermore, the protocol should include subjecting UV-aged plastics to microorganisms, such as those identified by Peixoto et al. (2022), to achieve controlled biodegradation. It is expected that intense photo-oxidation coupled with these alternative degradation methods will result in artificially aged films (or microparticles) more representative of those encountered in urban hydrosystems. The development of model plastic films representing environmentally aged presents opportunities for interdisciplinary research spanning ecology, materials science, fluid mechanics, and environmental sciences. While this study focused on PE, the approach could also be applied to other polymers and to a broader range of consumer products. It would be valuable to further characterize the degradation markers and kinetics of plastic objects used in everyday life. This study underscores the importance of in situ and laboratory-coupled approaches for addressing the complex challenges associated with plastic degradation and MP pollution.

Declarations

Acknowledgments. The authors would like to thank the OTHU more specifically Nicolas Walcker and Serge Naltchayan for their help to visit the detention basin and to collect samples and the Grand Lyon for agreeing to let visit the sites studied. The authors also thank the NMR Polymer platform of Institut de Chimie de Lyon (FR5223), and in special Carlos Fernandez de Alba Encinas, for assistance and access to the NMR facilities, Laura Courty of Ingenierie des Materiaux Polymères (IMP) for her assistance and help with the FTIR spectrometer. Finally the authors would like to thank Laurent Simon of Laboratoire d'Ecologie des Hydrosystèmes Naturels et Anthropisés (LEHNA) for his precious help and fruitful discussions.

Authors Contribution. All authors contributed to the study conception and design. Material preparation, investigation, data collection and formal analysis were performed by ZI and OM. VMN, EM, DL, GLK, RB and BM supervised the study. The original draft of the manuscript was written by ZI and OM, all authors reviewed and edited all previous versions of the manuscript. All authors read and approved the final manuscript.

Funding. This work was carried out thanks to the financial support of the University of Lyon's LabEx iMUST (ANR-10LABX-0064), as part of the "Programme d'Investissements d'Avenir" set up by the French government and managed by the "Agence Nationale de la Recherche" (ANR). This work has been supported by the Graduate School H2O'Lyon (ANR-17- EURE0018) of Université de Lyon (UdL), within the program "Investissements d'Avenir" operated by the French National Research Agency (ANR). This work has also been supported as well from INSA Lyon as part of Okba Mostefaoui's "INSA Lyon Environmental Issues" MESR thesis grant. The funding for Zoé Iannuzzi's internship as carried out within the framework of the Sedi-Plast research program (https://anr-sedi-plast.univ-gustave-eiffel.fr/) funded by the French Research Agency (ANR-19-CE34-0012), and finally the french MESR ministry for Zoé Iannuzzi's thesis grant.

Availability of data and materials. All raw spectra data that support the findings of this study are openly available in zenodo at http://doi.org/10.5281/zenodo.10578160.

Ethical Approval. This declaration is not applicable.

References

Albertsson, A.C., Andersson, S.O., Karlsson, S., 1987. The mechanism of biodegradation of polyethylene. Polymer degradation and stability 18, 73– 87. doi:10.1016/0141-3910(87)90084-X.

Almond, J., Sugumaar, P., Wenzel, M.N., Hill, G., Wallis, C., 2020. Determination of the carbonyl index of polyethylene and polypropylene using specified area under band methodology with atr-ftir spectroscopy. e-Polymers 20, 369–381. doi:10.1515/epoly-2020-0041.

Arp, H.P.H., Ku¨hnel, D., Rummel, C., MacLeod, M., Potthoff, A., Reichelt, S., Rojo-Nieto, E., Schmitt-Jansen, M., Sonnenberg, J., Toorman, E., et al., 2021. Weathering plastics as a planetary boundary threat: exposure, fate, and hazards. Environmental science & technology 55, 7246–7255. doi: 10.1021/acs.est.1c01512

Assink, R.A., Celina, M., Dunbar, T.D., Alam, T.M., Clough, R.L., Gillen, K.T., 2000. Analysis of hydroperoxides in solid polyethylene by mas 13c nmr and epr. Macromolecules 33, 4023–4029. doi:10.1021/ma991970d.

Banfi, D., Patiny, L., 2008. www. nmrdb. org: Resurrecting and processing nmr spectra on-line. Chimia 62, 280–280. doi:10.2533/chimia.2008.280.

Bhagat, K., Barrios, A.C., Rajwade, K., Kumar, A., Oswald, J., Apul, O., Perreault, F., 2022. Aging of microplastics increases their adsorption affinity towards organic contaminants. Chemosphere 298, 134238. doi:10.1016/j.chemosphere.2022.134238.

Bovey, F.A., Gooden, R., Schilling, F.C., Winslow, F.H., 1988. Carbon-13 nmr study of the solid-state photochemistry of poly (ethylene-co-carbon monoxide). Macromolecules 21, 938–944. doi:10.1021/ma00182a016.

Brandon, J., Goldstein, M., Ohman, M.D., 2016. Long-term aging and degradation of microplastic particles: Comparing in situ oceanic and experimental weathering patterns. Marine Pollution Bulletin 110, 299–308. doi:10.1016/j.marpolbul.2016.06.048.

Burrows, S., Colwell, J., Costanzo, S., Kaserzon, S., Okoffo, E., Ribeiro, F., ... & Galloway, T. (2024). UV sources and plastic composition influence microplastic surface degradation: Implications for plastic weathering studies. *Journal of Hazardous Materials Advances*, *14*, 100428. doi:10.1016/j.hazadv.2024.100428.

Cai, L., Wang, J., Peng, J., Wu, Z., Tan, X., 2018. Observation of the degradation of three types of plastic pellets exposed to uv irradiation in three different environments. Science of the Total Environment 628, 740– 747. doi:10.1016/j.scitotenv.2018.02.079.

Chen, Y., Awasthi, A. K., Wei, F., Tan, Q., & Li, J. (2021). Single-use plastics: Production, usage, disposal, and adverse impacts. Science of the total environment, 752, 141772. doi: 10.1016/j.scitotenv.2020.141772

Colomw, X., Canavate, J., Pagés, P., Saurina, J., & Carrasco, F. (2000). Changes in crystallinity of the HDPE matrix in composites with cellulosic fiber using DSC and FTIR. Journal of reinforced plastics and composites, 19(10), 818-830. doi:10.1177/073168440001901003

Cui, X., Yang, T., Li, Z., Nowack, B., 2024. Meta-analysis of the hazards of microplastics in freshwaters using species sensitivity distributions. Journal of Hazardous Materials 463, 132919. doi:10.1016/j.jhazmat.2023.132919.

Da Costa, J.P., Nunes, A.R., Santos, P.S., Girao, A.V., Duarte, A.C., RochaSantos, T., 2018. Degradation of polyethylene microplastics in seawater: Insights into the environmental degradation of polymers. Journal of Environmental Science and Health, Part A 53, 866–875. doi:10.1080/ 10934529.2018.1455381.

Dhivert, E., Pruvost, J., Winiarski, T., Gasperi, J., Delor-Jestin, F., Tassin, B., & Mourier, B. (2024). Time-varying microplastic contributions of a large urban and industrial area to river sediments. *Environmental Pollution*, 123702. doi: 10.1016/j.envpol.2024.123702

Duan, J., Bolan, N., Li, Y., Ding, S., Atugoda, T., Vithanage, M., Sarkar, B., Tsang, D.C., Kirkham, M., 2021. Weathering of microplastics and interaction with other coexisting constituents in terrestrial and aquatic environments. Water Research 196, 117011. doi:10.1016/j.watres.2021.117011.

Erni-Cassola, Gabriel, Zadjelovic, Vinko, Gibson, Matthew I & Christie-Oleza, Joseph A 2019 Distribution of plastic polymer types in the marine environment; a meta-analysis. Journal of hazardous materials 369, 691–698. doi: 10.1016/j.jhazmat.2019.02.067

European Commission, 2022. Photovoltaic geographical information system. URL: https://re.jrc.ec.europa.eu/pvg_tools/en/.

Fernando, S.S., Christensen, P.A., Egerton, T.A., White, J.R., 2007. Carbon dioxide evolution and carbonyl group development during photodegradation of polyethylene and

polypropylene. Polymer Degradation and Stability 92, 2163–2172. doi:10.1016/j.polymdegradstab.2007.01.032.

Gardette, M., Perthue, A., Gardette, J.L., Janecska, T., Fo¨ldes, E., Pukanszky, B., Therias, S., 2013. Photo- and thermal-oxidation of polyethylene: Comparison of mechanisms and influence of unsaturation content. Polymer Degradation and Stability 98, 2383–2390. doi:10.1016/ j.polymdegradstab.2013.07.017.

Gong, J., Xie, P., 2020. Research progress in sources, analytical methods, ecoenvironmental effects, and control measures of microplastics. Chemosphere 254, 126790. doi:10.1016/j.chemosphere.2020.126790.

Gulmine, J., Janissek, P., Heise, H., Akcelrud, L., 2003. Degradation profile of polyethylene after artificial accelerated weathering. Polymer degradation and stability 79, 385–397. doi:10.1016/S0141-3910(02)00338-5.

Hakkarainen, M., Albertsson, A.C., 2004. Environmental degradation of polyethylene. Long term properties of polyolefins , 177–200doi:10.1007/ b13523.

Han, S.O., Lee, D.W., Han, O.H., 1999. Thermal degradation of crosslinked high density polyethylene. Polymer degradation and stability 63, 237–243. doi:10.1016/S0141-3910(98)00098-6.

Hanun, J.N., Hassan, F., Jiang, J.J., 2021. Occurrence, fate, and sorption behavior of contaminants of emerging concern to microplastics: Influence of the weathering/aging process. Journal of Environmental Chemical Engineering 9, 106290. doi:10.1016/j.jece.2021.106290.

Hossain, M.B., Yu, J., Nur, A.A.U., Banik, P., Jolly, Y.N., Al-Mamun, M., Paray, B.A., Arai, T., 2023. Distribution, characterization and contamination risk assessment of microplastics in the sediment from the world's top sediment-laden estuary. Journal of Environmental Management 344, 118472. doi:10.1016/j.jenvman.2023.118472.

Hsu, Y. J., Huang, C., & Lee, M. (2024). Unveiling microplastic spectral signatures under weathering and digestive environments through shortwave infrared hyperspectral sensing. *Environmental Pollution*, *342*, 123106. doi:10.1016/j.envpol.2023.123106.

Huang, W., Deng, J., Liang, J., Xia, X., 2023. Comparison of lead adsorption on the aged conventional microplastics, biodegradable microplastics and environmentally-relevant tire wear particles. Chemical Engineering Journal 460, 141838. doi:10.1016/j.cej.2023.141838.

Hüffer, T., Weniger, A.K., Hofmann, T., 2018. Sorption of organic compounds by aged polystyrene microplastic particles. Environmental Pollution 236, 218–225. doi:10.1016/j.envpol.2018.01.022.

Iannuzzi, Z., Mourier, B., Winiarski, T., Lipeme-Kouyi, G., Polome, P., Bayard, R., 2024. Contribution of different land use catchments on the microplastic pollution in detention basin sediments. Environmental Pollution doi:10.1016/j.envpol.2024.123882.

Jelle, B.P., Nilsen, T.N., 2011. Comparison of accelerated climate ageing methods of polymer building materials by attenuated total reflectance Fourier transform infrared radiation spectroscopy. Construction and Building Materials 25, 2122–2132. doi:10.1016/j.conbuildmat.2010.11.020.

Kalogerakis, N., Karkanorachaki, K., Kalogerakis, G.C., Triantafyllidi, E.I., Gotsis, A.D., Partsinevelos, P., Fava, F., 2017. Microplastics generation: onset of fragmentation of polyethylene films in marine environment mesocosms. Frontiers in Marine Science 4, 84. doi:10.3389/fmars.2017.00084.

Karlsson, S., Albertsson, A.C., 2002. Techniques and mechanisms of polymer degradation, in: Degradable Polymers: Principles and Applications. Springer, pp. 51–69. doi:10.1007/978-94-017-1217-0_4.

Lacoste, J., Carlsson, D., 1992. Gamma-, photo-, and thermally-initiated oxidation of linear low density polyethylene: A quantitative comparison of oxidation products. Journal of Polymer Science Part A: Polymer Chemistry 30, 493–500. doi:10.1002/pola.1992.080300316.

Lambert, S., Wagner, M., 2016. Formation of microscopic particles during the degradation of different polymers. Chemosphere 161, 510–517. doi:10. 1016/j.chemosphere.2016.07.042.

Li, C., Li, X., Bank, M.S., Dong, T., Fang, J.K.H., Leusch, F.D., Rillig, M.C., Wang, J., Wang, L., Xia, Y., et al., 2024. The "microplastome"– a holistic perspective to capture the real-world ecology of microplastics. Environmental Science & Technology doi:10.1021/acs.est.3c08849.

Lin, J., Yan, D., Fu, J., Chen, Y., Ou, H., 2020. Ultraviolet-c and vacuum ultraviolet inducing surface degradation of microplastics. Water Research 186, 116360. doi:10.1016/j.watres.2020.116360.

Lipeme Kouyi, G., Barraud, S., Becouze-Lareure, C., Blaha, D., Perrodin, Y., Wiest, L., Aubin, J.B., Toussaint, J.Y., Vareilles, S., Mandon, C., et al., 2018. Characterization of and new management insights for sediments in a stormwater detention basin. Techniques Sciences Méthodes , 65– 75doi:10.1051/tsm/201809065.

Liu, G., Zhu, Z., Yang, Y., Sun, Y., Yu, F., Ma, J., 2019. Sorption behavior and mechanism of hydrophilic organic chemicals to virgin and aged microplastics in freshwater and seawater. Environmental Pollution 246, 26–33. doi:10.1016/j.envpol.2018.11.100.

Liu, P., Zhan, X., Wu, X., Li, J., Wang, H., Gao, S., 2020. Effect of weathering on environmental behavior of microplastics: Properties, sorption and potential risks. Chemosphere 242, 125193. doi:10.1016/j.chemosphere.2019.125193.

Luo, H., Zhao, Y., Li, Y., Xiang, Y., He, D., Pan, X., 2020. Aging of microplastics affects their surface properties, thermal decomposition, additives leaching and interactions in simulated fluids. Science of The Total Environment 714, 136862. doi:10.1016/j.scitotenv.2020.136862.

Maddams, W.F. and Parker, S.F. (1989), Vibrational spectroscopy of the oxidation of polyethylene. I. Fourier self-deconvolution of the carbonyl absorption. J. Polym. Sci. B Polym. Phys., 27: 1691-1698. doi:10.1002/polb.1989.090270808

Moreira, C., Lloyd, R., Hill, G., Huynh, F., Trufasila, A., Ly, F., Sawal, H., Wallis, C., 2021. Temperate uv-accelerated weathering cycle combined with ht-gpc analysis and drop point testing for determining the environmental instability of polyethylene films. Polymers 13, 2373. doi:10.3390/ polym13142373.

Nakajima, R., Tsuchiya, M., Lindsay, D.J., Kitahashi, T., Fujikura, K., Fukushima, T., 2019. A new small device made of glass for separating microplastics from marine and freshwater sediments. PeerJ 7, e7915. doi:10.7717/peerj.7915.

Oberbeckmann, S., Lo¨der, M.G., Labrenz, M., 2015. Marine microplasticassociated biofilms–a review. Environmental chemistry 12, 551–562. doi:10.1071/EN15069.

Ogihara, T., 1963. Oxidative degradation of polyethylene in nitrogen dioxide. Bulletin of the Chemical Society of Japan 36, 58–63. doi:10.1246/bcsj. 36.58.

Osterlund, H., Blecken, G., Lange, K., Marsalek, J., Gopinath, K., Viklander,¨ M., 2023. Microplastics in urban catchments: Review of sources, pathways, and entry into stormwater. Science of the Total Environment 858, 159781. doi:10.1016/j.scitotenv.2022.159781

Pavia, D.L., Lampman, G.M., Kriz, G.S., Vyvyan, J.A., 2014. Introduction to spectroscopy. Cengage Learning, Stamford, Connecticut, USA.

Peixoto, J., Vizzotto, C., Ramos, A., Alves, G., Steindorff, A., Kru¨ger, R., 2022. The role of nitrogen metabolism on polyethylene biodegradation. Journal of Hazardous Materials 432, 128682. doi:10.1002/ldr.4330.

Primpke, S., Wirth, M., Lorenz, C., Gerdts, G., 2018. Reference database design for the automated analysis of microplastic samples based on fourier transform infrared (ftir) spectroscopy. Analytical and bioanalytical chemistry 410, 5131–5141. doi:10.1007/s00216-018-1156-x.

Ramirez-Alvarez, N., Mendoza, L.M.R., Macias-Zamora, J.V., Oregel-Vazquez, L., Alvarez-Aguilar, A., Hernandez-Guzman, F.A., S´anchezOsorio, J.L., Moore, C.J., Silva-Jiménez, H.,

Navarro-Olache, L.F., 2020. Microplastics: Sources and distribution in surface waters and sediments of todos santos bay, mexico. Science of the Total Environment 703, 134838. doi:10.1016/j.scitotenv.2019.134838.

Sandt, C., Waeytens, J., Deniset-Besseau, A., Nielsen-Leroux, C., Réjasse, A., 2021. Use and misuse of ftir spectroscopy for studying the bio-oxidation of plastics. Spectrochimica Acta Part A: Molecular and Biomolecular Spectroscopy 258, 119841. doi:10.1016/j.saa.2021.119841.

Shen, X., Xu, L., Ye, S., Hu, R., Jin, L., Xu, H., Liu, W., 2018. Automatic baseline correction method for the open-path fourier transform infrared spectra by using simple iterative averaging. Optics express 26, A609–A614.
doi:10.1364/OE.26.00A609.

Socrates, G., 2004. Infrared and Raman characteristic group frequencies: tables and charts. John Wiley & Sons, Hoboken, New Jersey, USA.

Song, Y.K., Hong, S.H., Jang, M., Han, G.M., Jung, S.W., Shim, W.J., 2017. Combined effects of uv exposure duration and mechanical abrasion on microplastic fragmentation by polymer type. Environmental science & technology 51, 4368–4376. doi:0.1021/acs.est.6b06155.

Sorasan, C., Edo, C., Gonzalez-Pleiter, M., Fernandez-Pinas, F., Leganés, F., Rodrıguez, A., Rosal, R., 2022. Ageing and fragmentation of marine microplastics. Science of The Total Environment 827, 154438. doi:10. 1016/j.scitotenv.2022.154438.

Stark, N. M., & Matuana, L. M. (2004). Surface chemistry and mechanical property changes of wood-flour/high-density-polyethylene composites after accelerated weathering. *Journal of Applied Polymer Science*, *94*(6), 2263-2273. doi:10.1002/app.20996

Sun, Y., Yuan, J., Zhou, T., Zhao, Y., Yu, F., Ma, J., 2020. Laboratory simulation of microplastics weathering and its adsorption behaviors in an aqueous environment: a systematic review. Environmental pollution 265, 114864. doi:10.1016/j.envpol.2020.114864.

Sutherland, B.R., DiBenedetto, M., Kaminski, A., Van Den Bremer, T., 2023. Fluid dynamics challenges in predicting plastic pollution transport in the ocean: A perspective. Physical Review Fluids 8. doi:10.1103/ PhysRevFluids.8.070701.

Wang, C., Zhao, J., Xing, B., 2021a. Environmental source, fate, and toxicity of microplastics. Journal of hazardous materials 407, 124357. doi:10.1016/j.jhazmat.2020.124357.

Wang, G., Lu, J., Li, W., Ning, J., Zhou, L., Tong, Y., Liu, Z., Zhou, H., Xiayihazi, N., 2021b. Seasonal variation and risk assessment of microplastics in surface water of the manas river basin, china. Ecotoxicology and environmental safety 208, 111477. doi:10.1016/j.ecoenv.2020.111477.

Wang, J., Bucci, K., Helm, P., Hoellein, T., Hoffman, M., Rooney, R., Rochman, C., 2022. Runoff and discharge pathways of microplastics into freshwater ecosystems: A systematic review and meta-analysis. Facets. doi:10.1139/facets-2022-0140.

Wang, T., Ma, Y., Ji, R., 2021c. Aging processes of polyethylene mulch films and preparation of microplastics with environmental characteristics. Bulletin of Environmental Contamination and Toxicology 107, 736–740. doi:10.1007/s00128-020-02975-x.

Wang, W., Gao, H., Jin, S., Li, R., Na, G., 2019. The ecotoxicological effects of microplastics on aquatic food web, from primary producer to human: A review. Ecotoxicology and environmental safety 173, 110–117. doi:10.1016/j.ecoenv.2019.01.113.

Wilkinson, J., Hooda, P.S., Barker, J., Barton, S., Swinden, J., 2017. Occurrence, fate and transformation of emerging contaminants in water: An overarching review of the field. Environmental Pollution 231, 954–970. doi:10.1016/j.envpol.2017.08.032.

Winiarska, E., Jutel, M., Zemelka-Wiacek, M., 2024. The potential impact of nano-and microplastics on human health: Understanding human health risks. Environmental Research , 118535. doi:10.1016/j.envres.2024.118535.

Zerbi, G., Gallino, G., Del Fanti, N., & Baini, L. (1989). Structural depth profiling in polyethylene films by multiple internal reflection infra-red spectroscopy. Polymer, 30(12), 2324-2327. doi:10.1016/0032-3861(89)90269-3

Zhang, Y., Peng, Y., Xu, S., Zhang, S., Zhou, G., Yang, J., Li, H., Zhang, J., 2022. Distribution characteristics of microplastics in urban rivers in chengdu city: The influence of land-use type and population and related suggestions. Science of The Total Environment 846, 157411. doi:10.1016/ j.scitotenv.2022.157411.

Zhang, Z., Zou, S., Li, P., 2023. Aging of plastics in aquatic environments: Pathways, environmental behavior, ecological impacts, analyses and quantifications. Environmental Pollution , 122926doi:10.1016/j. envpol.2023.122926.

Zhu, K., Jia, H., Sun, Y., Dai, Y., Zhang, C., Guo, X., Wang, T., Zhu, L., 2020. Long-term phototransformation of microplastics under simulated sunlight irradiation in aquatic environments: Roles of reactive oxygen species. Water Research 173, 115564. doi:10.1016/j.watres.2020.115564.

Declaration of interests

☒ The authors declare that they have no known competing financial interests or personal relationships that could have appeared to influence the work reported in this paper.

☐ The authors declare the following financial interests/personal relationships which may be considered as potential competing interests:

Highlights

- In-situ microplastics exhibit elevated levels of both abiotic and biotic degradation
- Our protocol mimics the abiotic degradation observed in in-situ microplastics
- Comparable carbonyl index values are observed between in-situ and laboratory samples
- Carbonyl bonds persist as the predominant form in in-situ microplastics
- Critical degradation phases were identified during transfer in urban hydrosystems